Effective field theory of the zero-temperature triangular-lattice antiferromagnet: A Monte Carlo study

Hui Yin and Bulbul Chakraborty
The Martin Fisher School of Physics, Brandeis University, Waltham, Massachusetts 02454

Nicholas Gross
College of General Studies, Boston University, Boston, Massachusetts 02215
(Received 4 January 2000)

Using a Monte Carlo coarse-graining technique introduced by Binder [Z. Phys. B **43**, 119 (1981)], we have explicitly constructed the continuum field theory for the zero-temperature triangular Ising antiferromagnet. We verify the conjecture that this is a Gaussian theory of the height variable in the interface representation of the spin model. We also measure the height-height correlation function and deduce the stiffness constant. In addition, we investigate the nature of defect-defect interactions at finite temperatures, and find that the two-dimensional Coulomb gas scenario applies at low temperatures.

PACS number(s): 05.70.Jk, 05.50.+q, 05.10.Ln, 02.70.Lq

I. INTRODUCTION

In recent years, there has been considerable interest in the study of classical spin systems with critical ground states. One of the best studied of these is the triangular-lattice Ising antiferromagnet (TIAFM) [1]. The critical behavior of these models can be understood based on an interface representation and an ''effective'' field theory which is Gaussian in the height variable [2,3]. In this paper we present an explicit construction of the effective field theory based on the study of Monte Carlo cell distribution functions [4] of the TIAFM. To accomplish this, a height mapping [5] is applied to the system and this variable is then coarse grained to obtain a continuum field theory. Our interest in this model was stimulated by the observation of anomalously slow dynamics in the compressible TIAFM [6]. In that model the supercooled state exhibits an ergodicity-breaking transition which is reminiscent of the structural-glass transition. This glassy behavior is believed to arise from the interaction between strings and vortices [7], the topological defects present in these models at finite temperature. In the pure TIAFM model, the Gaussian theory implies that the vortices interact as charges of a two-dimensional (2D) Coulomb gas [8]. We have analyzed the defect-defect correlation function at finite temperatures to investigate the nature of the defect interactions. The 2D simulations are consistent with the Coulomb gas picture at low densities of defects.

The motivation behind this numerical study was (1) to test the Monte Carlo cell distribution function technique in a model where the effective field theory is well established and (2) to establish a framework for the construction of effective field theories and effective defect-defect interactions in models such as the compressible TIAFM where no adequate field theory description exists.

The paper is organized as follows. In Sec. II we describe the cell distribution function technique. In Sec. III we present results from the coarse-grained free-energy functional and compare our results to the Gaussian theory. In Sec. IV we verify the Gaussian theory from a study of the height-height correlation function and in Sec. V we describe the study of the defect-defect correlation functions. Section VI presents our conclusions and directions for future work.

II. CELL DISTRIBUTION FUNCTIONS AND COARSE-GRAINED FREE-ENERGY FUNCTIONALS

Kaski, Binder, and Gunton [9,10] have studied cell distribution functions of the three-dimensional Ising model on a cubic lattice and constructed coarse-grained Ginzburg-Landau Hamiltonians. In this section we review this technique and present the results of its application to the triangular Ising ferromagnet as an example. We will describe the application of this technique to the zero-temperature TIAFM in Sec. III.

Given a microscopic Hamiltonian such as the Ising model, Monte Carlo (MC) methods can be used to sample the distribution functions $P_L(\{s_i\})$ of the coarse-grained variables

$$s_i = \frac{1}{L^2} \sum_{l \in i^{th}} S_l ,$$

where S_l are the original microscopic spin variables, such as the Ising spins on the original lattice, and L is the cell size. The distributions $P_L(\{s_i\})$ are assumed to be of the form $e^{-\beta \mathcal{F}}$ with $\mathcal{F}$ having the Ginzburg-Landau (GL) form in terms of the coarse-grained variables $\{s_i\}$. This assumption is expected to be valid when $L \gg a$ (lattice spacing) but much smaller than the correlation length, such that the coarse-grained variables do not fluctuate rapidly from cell to cell. If one could sample the total distribution function in MC simulations, then this connection could be exploited for the explicit construction of the GL Hamiltonian by simulating the microscopic model. Sampling the total distribution function is essentially an impossible task and therefore, we have followed Binder [10] in studying the two simplest reduced distribution functions, the single cell and the joint, nearest-neighbor, two-cell distribution functions which are then parametrized by the GL form. To illustrate how the cell distribution function method works, we briefly describe its ap-

plication to the triangular Ising ferromagnet in zero magnetic field, where we choose the model system size to be 80×80 with periodic boundary conditions and the cell sizes L to be 4, 8, 10, 16, 20, and 40.

The microscopic Hamiltonian is

$$\mathcal{H}_{\mathrm{Ising}}=-J\sum_{\substack{l\neq l'\\ \langle ll'\rangle}} S_l S_{l'}\,.$$

The total distribution function $P_L(\{s_i\})$ is assumed to be

$$P_L(\{s_i\})=\frac{1}{Z}e^{-\mathcal{F}_{GL}(\{s_i\})}, \tag{1}$$

where Z is the partition function and the GL Hamiltonian has the form

$$\mathcal{F}_{GL}(\{s_i\})=\sum_i\ (\overline{r_L}s_i^2+\overline{u_L}s_i^4)+\sum_{\langle ij\rangle}\overline{c_L}(s_i-s_j)^2. \tag{2}$$

The two reduced distribution functions, which are amenable to numerical calculations, are the two-cell joint distribution function $P_L(s_i,s_j)$ and the single-cell distribution function $P_L(s_i)$,

$$P_L(s_i,s_j)=\int\prod_{\substack{l\neq i\\ l\neq j\\ \langle ij\rangle}} ds_l P_L(\{s_l\}), \tag{3}$$

$$P_L(s_i)=\int P_L(s_i,s_j)ds_j\,. \tag{4}$$

The parametrization of the effective Hamiltonian is accomplished by sampling $P_L(s_i,s_j)$ and $P_L(s_i)$,

$$P_L(s_i,s_j)=\frac{1}{Z'}\exp\{-[c_L(s_i-s_j)^2+V_L(s_i)+V_L(s_j)]\}, \tag{5}$$

$$P_L(s_i)=\frac{1}{Z''}e^{-V_L(s_i)}, \tag{6}$$

where Z' and Z'' are normalization factors, and

$$V_L(s_i)=r_L s_i^2+u_L s_i^4. \tag{7}$$

The r_L and u_L obtained from $P_L(s_i,s_j)$ and $P_L(s_i)$, respectively, can be different since the effect of the gradient term has been integrated over in the single-cell distribution function. Similar considerations imply that these coefficients can be different from $\overline{r_L}$, $\overline{u_L}$, and $\overline{c_L}$ in Eq. (2). For small values of $\overline{c_L}$, the coupling between different sites is small and all of these coefficients are expected to be approximately equal [10]. The coefficients r_L, u_L, and c_L, as functions of temperature (T) and cell size (L), can be estimated by fitting the measured distribution function $P_L(s_i,s_j)$ to the model form [Eq. (5)]. It is well known that a temperature-driven second order transition exists for this Ising model and the exact result for $T_c(\infty)=3.6$ [11]. Figure 1 shows $r_L(T)/u_L(T)$ as a function of temperature for different cell sizes. There is clear evidence for a temperature-driven second order transition at

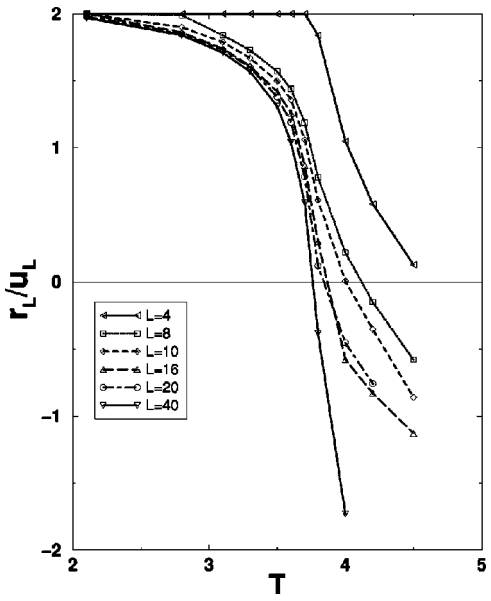

FIG. 1. The ratio $r_L(T)/u_L(T)$, calculated from the joint distribution function for different cell sizes. $T_c(L)$ is identified as the point where $r_L/u_L=0$. The exact result for $T_c(\infty)$ is 3.6 [11]. The temperature is plotted in units of J/k_B and r_L/u_L is dimensionless [cf. Eqs. (5) and (7)].

$T_c(L)$ where the sign of the ratio changes. The L dependence of $T_c(L)$ agrees with finite size scaling predictions [4]. The variation of $c_L(T)/u_L(T)$ with cell size L (Fig. 2) shows temperature-dependent behavior as the size of the cells approach infinity. For temperatures above $T_c(\infty)$, the ratio ap-

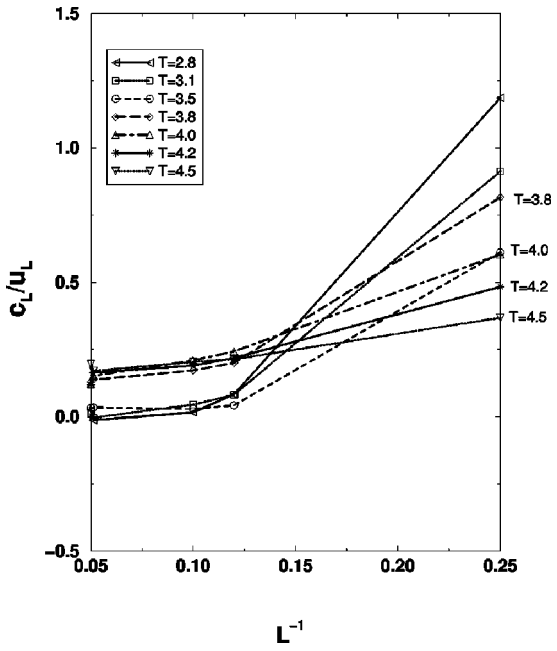

FIG. 2. The ratio $c_L(T)/u_L(T)$, calculated from the joint distribution function for different temperatures, plotted as a function of L^{-1}. The length is measured in units of the lattice spacing and c_L/u_L is dimensionless. The curves can be divided into two groups. For those with temperatures higher than $T_c(\infty)=3.6$ (identified in the figure), the curves converge to a finite value. For those with temperatures lower than $T_c(\infty)$, the curves converge to zero.

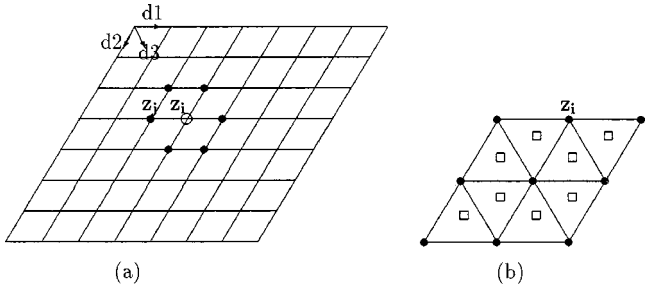

FIG. 3. (a) The three nearest-neighbor directions d_1, d_2, d_3, and the six nearest neighbors (black dots) of discrete height variables z_i (open circle) mapped onto the rhombus-shaped lattice used in the simulation. (b) The coarse-graining cell of size $L=2$. The vertices (black dots) of lattice are $\{z_i\}$ and the centers of the triangular plaquettes (open square) are $\{H_\mu\}$, each of which is defined as the average of the three surrounding z_i variables. The coarse-grained height variable h_l is defined as the average of all the H_μ variables within this cell.

proaches a nonzero fixed point as L approaches infinity. For all other temperatures, this ratio approaches zero. The sampling of the single-cell distribution function $P_L(s_i)$ [Eq. (6)] leads to similar results for r_L and u_L, which is consistent with the small value obtained for c_L. These results support the assumptions that went into the construction of $\mathcal{F}_{GL}(\{s_i\})$.

The results of this section will be contrasted with the frustrated antiferromagnetic case in Sec. III. The application of the distribution-function technique to the TIAFM is based on the mapping to an interface model and height variables. The coarse graining of these height variables and the GL parametrization are described in Sec. III.

III. RESULTS OF COARSE GRAINING AND COMPARISON WITH THE GAUSSIAN THEORY

A. Height variables and coarse graining at $T=0$

One interesting property of the TIAFM is that the ground state ensemble has a one-to-one mapping onto an interface model [2,3,5]. This provides a simple way of studying the properties of zero-temperature TIAFM.

The discrete variables in the interface model are height variables $\{z_l\}$, which are defined on each site of the triangular lattice. The mapping from the TIAFM to an interface model is realized by the mapping from spin variables $\{S_l\}$ to height variables $\{z_l\}$. Specifying the height variable to be zero at a chosen site, the following rules (Fig. 3) provide a unique mapping from $\{S_l\}$ to $\{z_l\}$.

(1) Along the d_1 direction, $\Delta z=-1$ for opposite spins and $\Delta z=+2$ for same spins.

(2) Along the d_2 direction, $\Delta z=-1$ for opposite spins and $\Delta z=+2$ for same spins.

(3) Along the d_3 direction, $\Delta z=+1$ for opposite spins and $\Delta z=-2$ for same spins.

These height assignments are unique up to the choice of origin as long as we restrict ourselves to Ising configurations in the ground state ensemble, which is the set of states that do not have any completely frustrated plaquettes (all spins are the same). The microscopic Hamiltonian in terms of these height variables $\{z_l\}$ can be written directly from the mapping as [2]

$$\mathcal{H}\{z_l\}=-J\sum_{\langle ij\rangle}(3-2|z_i-z_j|).$$

The symmetries of the original Hamiltonian are reflected in $\mathcal{H}\{z_l\}$. These include Ising up-down symmetry and sublattice symmetry. In addition, $\mathcal{H}\{z_l\}$ has a symmetry with respect to global, discrete shifts of the height variable. A detailed discussion of these symmetries can be found in Blöte and Nightingale [3]. An interesting property of this mapping is that for any ground state the height variable modulo 3 is the same for all spins on the same sublattice.

Starting from $\{z_l\}$, we can define a new set of height variables $\{H_\mu\}$ that are situated on the dual lattice, by averaging the three neighboring z_l on each triangular plaquette: $H_\mu=\frac{1}{3}(z_1+z_2+z_3)$ where z_1, z_2, and z_3 are on the three vertices of the μth plaquette [12] as shown in Fig. 3. Since the sum of z_1, z_2, and z_3 are multiples of 3, the $\{H_\mu\}$ is a set of integers.

We apply the coarse-graining technique to the height variables $\{H_\mu\}$. The coarse-graining cell is chosen to be a rhombus with the linear size L and the coarse-grained height variables $\{h_i\}$ are defined as the average of all the H_μ within the cell,

$$h_i=\frac{1}{N}\sum_{\mu\in i^{th}}H_\mu,$$

where N is the total number of H_μ variables within the ith cell. The coarse-graining cell is depicted schematically in Fig. 3. As L approaches infinity, the $\{h_i\}$ become continuous variables. The effective field theory is based on these continuous variables $\{h_i\}$, which describe the roughness of the interface. In the rough phase of the interface model, the average tilt of the interface, which is defined as the difference between $\langle h_m\rangle$ and $\langle h_n\rangle$ with the mth cell and the nth cell separated by the system size, is zero. For an arbitrary spin configuration, a tilt can be frozen in [5]. We will avoid such configurations in our simulations. Also $\{\langle h_i\rangle\}$ may be nonzero for a general choice of height origin and the Hamiltonian should only depend on the fluctuation $h_i-\langle h_i\rangle$ [5].

We performed Monte Carlo simulations on a system of size 600×600 shaped as a rhombus and looked at cell sizes 10, 15, 20, 30, 40, 50, 60, 75, and 100. We set the initial configuration to be one of the flat states [12], where $\{H_\mu\}$ is uniform in space. The dynamics we use in the simulation is single spin-flip Metropolis algorithm at zero temperature, where the energy is not allowed to increase and thus not all spins are flippable. The first 20 000 configurations are discarded to ensure that measurements are taken in equilibrium. The time independence of average quantities such as the staggered magnetization was used as evidence that the system has relaxed to its equilibrium state. The sampling is done every ten MC steps and for a total of 6000 configurations. Since we use single spin-flip MC dynamics, the average tilt is unchanged from its initial value of zero during the MC runs [13]. In the following sections, we will use h_i to represent $h_i-\langle h_i\rangle$.

B. Results and comparison with the Gaussian theory

It has been conjectured [2,3] that in terms of the height variables, the continuum theory for the zero temperature TIAFM is Gaussian,

$$\mathcal{F}(h(\vec{r}))=\int d\vec{r}\frac{\overline{c}}{2}[\nabla h(\vec{r})]^2 \tag{8}$$

with a value of $\overline{c}=\pi/9$. This stiffness constant was identified by Blöte *et al.* [5] through the correspondence between the exact calculation of the spin-spin correlation function in the spin model [14] and the discrete height-height correlation function in real space in the interface model [5]. The stiffness constant was also obtained numerically by Zeng and Henley from measurements of the discrete height correlation function in Fourier space [12]. In this section we deduce the stiffness constant by an explicit construction of the coarse-grained free energy.

Assuming a Ginzburg-Landau form for the Hamiltonian in terms of the continuous height variables,

$$\mathcal{F}(h(\vec{r}))=\int d\vec{r}\left\{\frac{\overline{a}}{2}h(\vec{r})^2+\frac{\overline{c}}{2}[\nabla h(\vec{r})]^2\right\}, \tag{9}$$

we proceed to obtain $\overline{a}$ and $\overline{c}$ from our simulations by parametrizing the joint distribution function of the coarse-grained height variables $P_L(h_i,h_j)$.

As in the triangular ferromagnet, we study the nearest-neighbor joint distribution function of heights,

$$P_L(h_i,h_j)=\int\prod_{\substack{l\neq i\\ l\neq j\\ \langle ij\rangle}} dh_l P_L(\{h_l\}), \tag{10}$$

where $P_L(\{h_l\})$ is the total cell distribution function. We parametrize the joint distribution function as

$$P_L(h_i,h_j)=\frac{1}{Z'}\exp\{-[c_L(h_i-h_j)^2+a_L(h_i^2+h_j^2)]\}, \tag{11}$$

where Z' is a normalization factor.

Anticipating a critical point at $T=0$, where $a_L\to 0$, we have neglected the quartic term in Eq. (11). This will be justified *a posteriori* from our numerical study. From the joint distribution function, we can extract a_L and c_L as in the ferromagnetic Ising model.

We examine a typical $P_L(h,h^*)$ for cell size $L=50$. One-dimensional cuts of $P_L(h_i,h_j)$ at different fixed values $h_j=h^*$ are shown in Fig. 4. The peak and shape of the cuts can be deduced from the distribution function [Eq. (11)] which is a product of two Gaussians, $\exp(-a_Lh^2)$ and $\exp[-c_L(h-h^*)^2]$. When h^* differs from 0 by a large amount, the plots in Fig. 4 show that the actual peak of the cut is much closer to h^* than to 0, which implies that the $\exp[-c_L(h-h^*)^2]$ is the dominant term in the product of Gaussians and the $\exp(-a_Lh^2)$ term acts more as a prefactor modulating the amplitude of the peak. The width of the cut is also seen to be determined mainly by c_L. Figure 4 indicates that a_L is small compared with c_L. We also analyze the importance of higher order gradient terms by measuring the non-Gaussian parameter (g_L) in the distribution of $v=\frac{1}{2}(h_i-h_j)$,

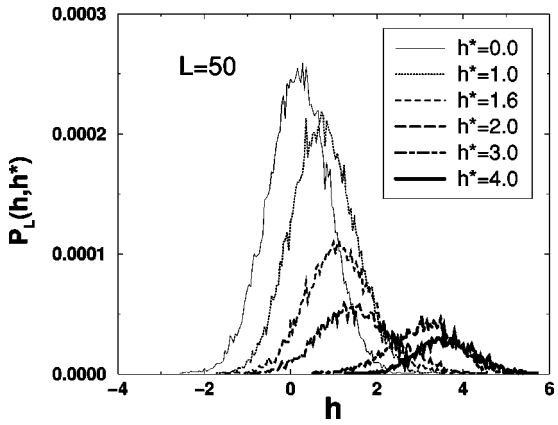

FIG. 4. The cuts of the probability distribution $P_L(h,h^*)$ for cell size $L=50$ and different values of h^*, demonstrating the dominance of the gradient term (cf. text). The height h is a dimensionless quantity.

$$g_L\equiv 1-\frac{\langle v^4\rangle_L}{3\langle v^2\rangle_L^2}. \tag{12}$$

We find g_L to be much smaller than 1, which is consistent with the assumed form of the gradient term in the joint distribution function. Extracting quantitative information about the coefficients a_L and c_L from fits to the distribution functions turns out to be difficult because of the essential two-dimensional nature of the distribution function $P_L(h_i,h_j)$ (c_L is large). Instead, we resort to measurement of moments for extracting quantitative information.

The parameters a_L and c_L can be related to the moments of $\{h_i\}$. We have calculated various moments of these coarse-grained variables directly from the MC simulations. In general, the parametrization of the joint distribution function [such as Eq. (11)] provides a connection between these moments and the coefficients of the GL Hamiltonian. For the model of Eq. (11), the relation between a_L and c_L and the moments can be shown to be

$$a_L=\frac{1}{2(\langle h^2\rangle+\langle h_1h_2\rangle)}, \tag{13}$$

$$c_L=\frac{\langle h_1h_2\rangle}{2(\langle h^2\rangle+\langle h_1h_2\rangle)(\langle h^2\rangle-\langle h_1h_2\rangle)}, \tag{14}$$

implying that

$$\frac{c_L}{a_L}=\frac{\langle h_1h_2\rangle}{(\langle h^2\rangle-\langle h_1h_2\rangle)}. \tag{15}$$

Here h_1 and h_2 refer to coarse-grained height variables on nearest-neighbor cells separated by the coarse-graining cell size L. These relations, between the parameters a_L and c_L and the moments, also provide the connection between a_L and c_L and the corresponding parameters $\overline{a}$ and $\overline{c}$ in continuum field theories such as in Eq. (9). Using the known

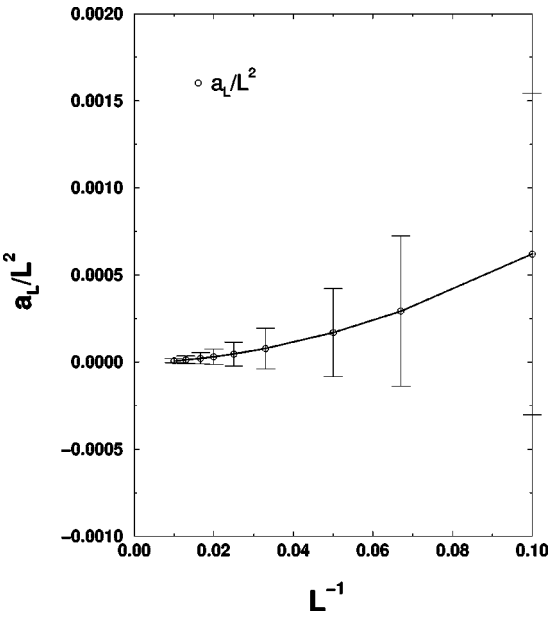

FIG. 5. Plots of $\overline{a_L}=a_L/L^2$ for different cell sizes. The open circles are the data points and the solid line is the second degree polynomial fit. The error bars are obtained from the standard deviations calculated from appropriate higher moments of h_i and h_j. The fitting of a_L/L^2 leads to a constant term with a value of 6.183E-6, which implies that the quadratic term in the field theory $\overline{a}$ [cf. Eq. (16)] becomes vanishingly small as $L\to\infty$. The length is measured in units of the lattice spacing and a_L is dimensionless.

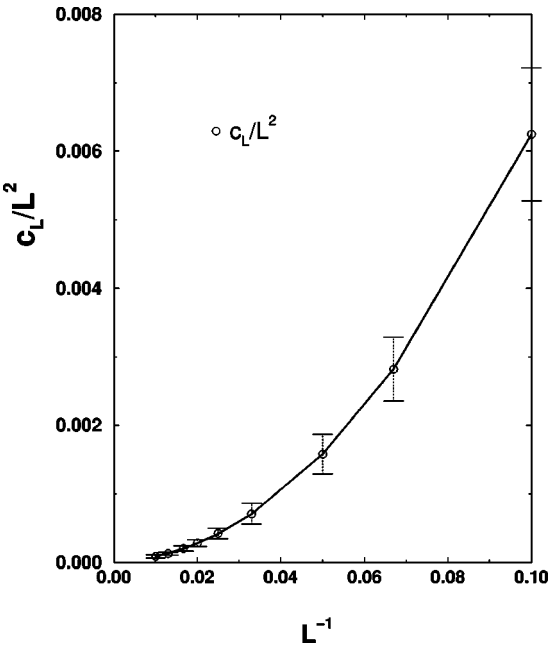

FIG. 6. Plots of c_L/L^2 for different cell sizes. The open circles are the data points and the solid line is the second degree polynomial fit. The error bars are the standard deviations calculated from appropriate higher moments of h_i and h_j. The fitting of c_L/L^2 leads to a quadratic term with a coefficient 0.622, and vanishingly small constant and linear terms, which implies that the gradient term of the continuous theory [cf. Eq. (17)], $\overline{c}$ approaches 0.392 as $L\to\infty$. The length is measured in units of the lattice spacing and c_L is dimensionless.

expressions for the correlations functions in the continuum model in two dimensions [15], these relations are

$$\overline{a}=4a_L L^{-2} \tag{16}$$

and

$$\overline{c}=2w_0\frac{\ln(\pi)}{\pi}c_L. \tag{17}$$

The factor $w_0=\sqrt{3}/2$ arises from the volume per unit cell in the triangular lattice. The prediction from the Gaussian theory is $\overline{a}=0$ and $\overline{c}=\pi/9$. We expect that, if the Gaussian theory is correct, then $\overline{a}$ should approach zero and $\overline{c}$ should remain constant as $L\to\infty$. Because of the connection to the continuum theory [Eq. (16)], it is natural to fit a_L/L^2 to a second-order polynomial in $1/L$. The results of the fitting are shown in Fig. 5. The value of $\overline{a}$ can be deduced from the constant term extracted from the fitting and is found to be 6.183×10^{-6}, implying that the quadratic term in the Ginzburg-Landau Hamiltonian becomes negligible as $L\to\infty$. It is difficult to extract the value of $\overline{c}$ from the measured values of c_L because of the fact that the errors increase with L [16]. If, instead, we analyze c_L/L^2, the error bars actually decrease with $1/L$ as seen from Fig. 6, and this provides a more precise way of determining the value of $\overline{c}$. As shown in Fig. 6, the data for c_L/L^2 can be fit very well to a second-order polynomial in $1/L$ with vanishingly small coefficients of the constant and linear term in $1/L$. The value of c_L obtained from this fit is 0.622. The standard deviations, calculated from the appropriate higher moments of h_i and h_j, based on Eqs. (13) and (14), are plotted as error bars.

These results for the parameters obtained from our analysis of the moments are completely consistent with the qualitative behavior deduced from the joint distribution functions, $P_L(h_i,h_j)$, shown in Fig. 4.

The results shown in Figs. 5 and 6 verify the Gaussian nature of the continuum theory. The numerical value of $\overline{c}$ extracted by applying Eq. (17) to the fitted value of c_L is 0.392, which is in very good agreement with the conjectured stiffness constant of $\pi/9=0.349$ [2,3].

IV. HEIGHT-HEIGHT CORRELATION FUNCTION

In this section we will briefly present our calculation of the correlation function of height variables in Fourier space, i.e., the power spectrum of the height variable, which can be used to deduce the stiffness constant as in the investigation of Zeng and Henley [12]. In Sec. V we further extend this technique to study the defect-defect interactions at finite temperatures by measuring the defect density correlation function.

As implied by Eq. (8), the stiffness constant $\overline{c}$ of the interface model can be directly related to the correlation function of height variables $\{h_i\}$ in Fourier space,

$$\mathcal{F}(h(\vec{r}))=\int d\vec{r}\frac{\overline{c}}{2}[\nabla h(\vec{r})]^2=\sum_{\vec{q}}\frac{\overline{c}}{2}|\vec{q}|^2|h(\vec{q})|^2. \tag{18}$$

Thus, the correlation function $\langle|h(\vec{q})|^2\rangle$ is

$$\langle |h(\vec{q})|^2 \rangle = \frac{1}{\overline{c}|\vec{q}|^2}. \tag{19}$$

The stiffness constant $\overline{c}$ can be extracted from a knowledge of $\langle |h(\vec{q})|^2 \rangle$. Numerical measurements of $\langle |h(\vec{q})|^2 \rangle$ are, however, arduous, and instead, we study the correlation function of the discrete height variables, $\langle |H(\vec{q})|^2 \rangle$, which should resemble $\langle |h(\vec{q})|^2 \rangle$ for small q except for a factor of $\sqrt{3}/2$ coming from the volume per lattice site. Therefore, the $\langle |H(\vec{q})|^2 \rangle$ for small q can be written as

$$\langle |H(\vec{q})|^2 \rangle = \frac{1}{c|\vec{q}|^2}, \tag{20}$$

where

$$c = \frac{2}{\sqrt{3}}\overline{c}. \tag{21}$$

We simulate a system of size 240×240. We start with the same flat states as the ones used in the coarse-graining simulations. After discarding the first 20 000 configurations and, again, ensuring that equilibrium has been reached, the simulations are sampled at every 10 MC steps for a total of 8000 configurations. For each sampled configuration we calculate $|H(\vec{q})|$, the two-dimensional Fourier transform of the discrete height variables $\{H_\mu\}$ (cf. Sec. III A) and average $|H(\vec{q})|^2$ over the sampled MC configurations.

For simplicity, one-dimensional cuts of $\langle |H(\vec{q})|^2 \rangle^{-1}$ along different directions in q space are shown in Fig. 7. As seen from Fig. 7, different cuts collapse on top of one another only for small values of q^2. This is due to the fact that the correlation function is isotropic for small values of q because of the sixfold rotational symmetry of the triangular lattice. As seen from the inset, the anisotropy starts to be significant when $q^2 > 1.6$. We have fitted $\langle |H(\vec{q})|^2 \rangle^{-1}$ to a second-order polynomial in q^2, restricting the fitting region to $q^2 < 0.2$. A value of $c = 0.414 \pm 0.016$ was extracted from the linear term of the fit. The nonlinear terms were small, and an estimate of the error on c was obtained from the standard deviation of the linear term extracted from fits to different segments of the curves ($q^2 < 0.2$). From Eq. (21), the stiffness constant can be deduced to be $\overline{c} = 0.360$, compared with 0.392 from our previous real space coarse-graining approach and $\pi/9 = 0.349$ from Blöte and Hilhorst [5].

The similarity of the results obtained from the real-space analysis and the power-spectrum analysis is quite remarkable and underlines the strength of these numerical techniques. A comparison of the two different analysis techniques, however, makes it clear that the power-spectrum analysis is simpler to implement and is the more desirable technique. The question of how well either of these techniques will fare when applied to a model with general nonlinear interactions, where very little is known analytically, is still open.

V. DEFECT INTERACTIONS

At finite temperatures, there are completely frustrated plaquettes which can be viewed as vortex excitations in the height variable [2,3]. There are two types of vortices corresponding to the two different orientations of the frustrated triangular plaquettes. These vortex excitations interact like charges via a two-dimensional Coulomb potential [3,8].

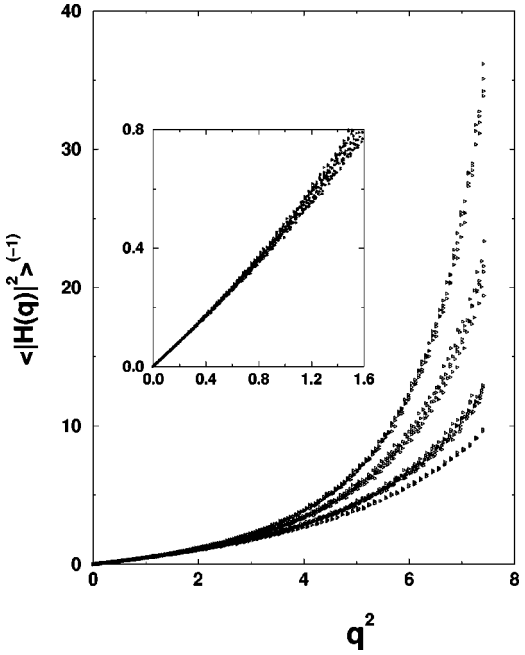

FIG. 7. Plots of $\langle |H(\vec{q})|^2 \rangle^{-1}$ vs $|\vec{q}|^2$. Different data sets are from the cuts of two-dimensional data along different directions in q space. The correlation function shows significant anisotropy for $q^2 \geq 1.6$. The value of $c = 0.414 \pm 0.016$ is obtained from the fitting of curves in the region $q^2 < 0.2$ to a second-degree polynomial in q^2. The stiffness constant $\overline{c}$ deduced from this fit is 0.360. The wave vector q is measured in units of the inverse lattice spacing and $H(\vec{q})$ is dimensionless.

An alternative to the Gaussian description is, therefore, a Coulomb gas description involving electric and magnetic charges corresponding to spin waves and vortices, respectively [3,8]. This connection suggests that extracting effective defect-defect interactions could be an alternative to constructing coarse-grained free energies. In complicated models and especially in analyzing dynamics, this might be the more viable alternative. We therefore wanted to numerically extract the effective vortex-vortex interaction in the TIAFM and verify the Coulomb gas scenario.

In the regime of low defect density, where mean field theory is expected to hold, the effective interactions can be related to the density-density correlation function [17]. The appropriate mean-field theory for our system with positive and negative charges is Debye-Hückle theory [17] which predicts that the charge-density correlation function has the following form:

$$\langle |\rho(q)|^2 \rangle = \frac{\kappa^2}{4\pi} \frac{q^2}{q^2 + \kappa^2}, \tag{22}$$

where

$$\kappa^2 = 4\pi(\langle n_+ \rangle + \langle n_- \rangle) \tag{23}$$

is the square of an inverse Debye-Hückle screening length. $\langle n_\pm \rangle$ are the average densities of positive and negative

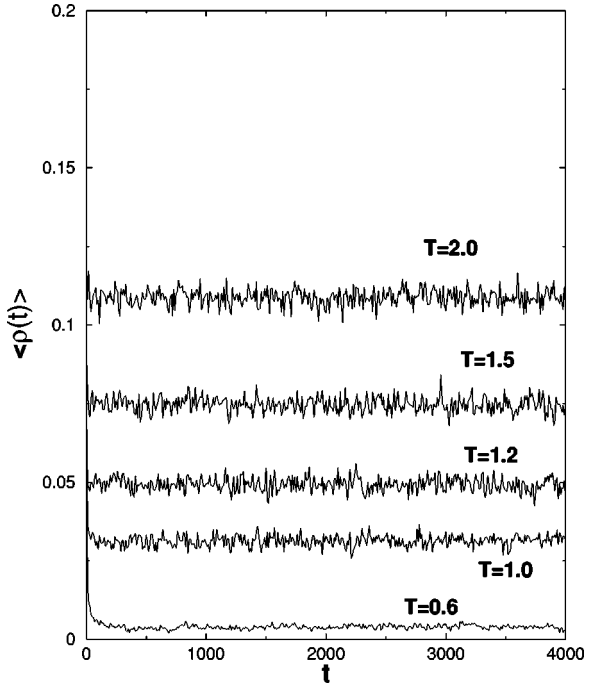

FIG. 8. The relaxation of defect (number) density in the first 4000 MC steps at different temperatures. As seen from the plots, defect densities relax to their equilibrium values by 4000 MC steps and fluctuate around it. The average defect density is 0.003, 0.030, 0.051, 0.0781, and 0.110, respectively, for $T=0.6$, 1.0, 1.2, 1.5, and 2.0. The defect density is dimensionless and the time is measured in units of Monte Carlo steps.

charges and $\rho(q)=n_+(q)-n_-(q)$, where $n_\pm(q)$ are the Fourier transform of the real space charge density functions.

If the vortices in our model behave as a Coulomb gas, then we expect to find this behavior of the charge-density correlation function at low temperatures where the vortex density is low.

We studied the charge density correlation function in a manner similar to that employed in the preceding section for studying the height-height correlation function. The MC simulations were performed on a 120×120 system and after discarding the first 10 000 configurations, samples were taken every five configurations. Figure 8 shows the typical defect density relaxations at different temperatures investigated in MC and it is clear that the time scale we choose to equilibrate the system is adequate. The correlation function, $\langle|\rho(q)|^2\rangle$, was measured at several temperatures.

The simulation results are shown in Fig. 9 along with the fits to the Debye-Hückle form [Eq. (22)]. The figure shows a one-dimensional cut of $\langle|\rho(q)|^2\rangle$ along a particular direction. In contrast to the height power spectrum, the defect density power spectrum was found to be isotropic within the range of q studied. The Debye-Hückle theory models the data well for all temperatures except the lowest temperature, $T=0.6$, which is shown in the inset. The lowest temperature data is suspect because the defect density is low and statistics are difficult to obtain. The isotropy of the $\langle|\rho(q)|^2\rangle$ data imply that the screening length and, therefore, the interactions between the defects on the triangular lattice is isotropic down to length scales of the order of the lattice spacing.

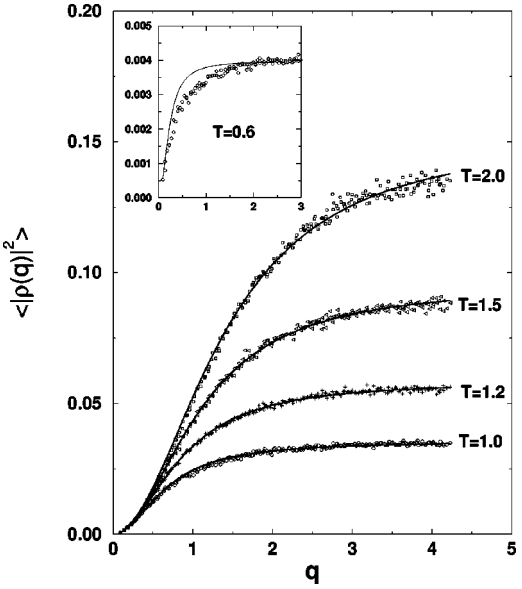

FIG. 9. Plots of the charge density correlation function at $T=1.0$, 1.2, 1.5, and 2.0. The data points are taken from cuts of two-dimensional data along one chosen direction since we did not observe any anisotropy (cf. text), and the solid lines are from the fittings to a Debye-Hückle form [Eq. (22)]. The fittings lead to κ_f^2 at different temperatures. The κ_f^2 and the analytical values of κ_a^2 extracted from the total defect density for the same temperature [cf. Eq. (23)] are shown in Fig. 10. The inset shows the fitting at the lowest temperature, $T=0.6$, where the defect density is 0.003 and the results suffer from a lack of statistics. The correlation function $\langle|\rho(q)|^2\rangle$ is dimensionless and q is measured in units of the inverse lattice spacing.

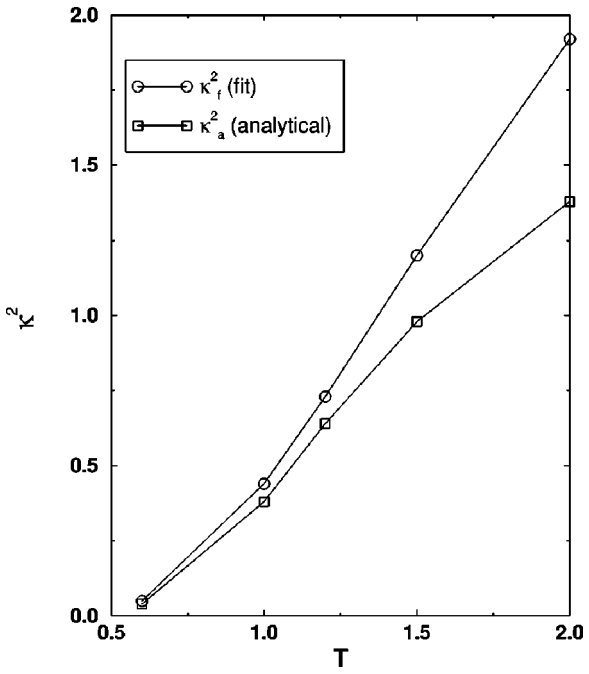

FIG. 10. Plots of κ_f^2, the inverse screening length obtained from fitting compared to κ_a^2, the value obtained from Eq. (23). The two curves deviate significantly only at the highest temperature where the defect picture itself starts to break down (cf. text). The screening length is measured in units of the lattice spacing and T is measured in units of J/k_B.

From the fits to the Debye-Hückle theory the inverse square of the screening length κ^2 can be extracted and compared to the analytic form given in Eq. (23), which uses as an input the measured defect density. In Fig. 10, the fitted values κ_f^2 and the analytic values κ_a^2 are plotted versus temperature. Except at the highest temperature, $T=2.0$, the agreement between the two different estimates is very good. Interestingly, the temperature at which the two κ's differ significantly from each other is also where the defect density differs from a simple Arrhenius prediction corresponding to an activation energy of $4J$, the single-defect creation energy. The observation of the large defect density at $T=2.0$, $\langle n_+ \rangle + \langle n_- \rangle = 0.110$, indicates that the defects are covering the whole lattice at this temperature and the single-defect picture becomes inappropriate.

These numerical studies show that it is possible to extract effective defect-defect interactions from measurements of the defect-density power spectrum and verifies that the interaction, in the TIAFM, is Coulombic. A numerical measurement of the force between defects has been made via a study of the dynamics of the defects in TIAFM [18]. This study could not confirm the existence of a Coulomb force from the behavior of the defect density at long times; however, it was argued that the force could not be falling off more slowly than $1/r$.

VI. CONCLUSION

Based on a mapping to an interface model, we have constructed a coarse-grained Hamiltonian for the zero-temperature TIAFM by studying the joint distribution function of the coarse-grained height variables. Our numerical work confirms that the effective field theory is Gaussian in terms of the coarse-grained height variables and we obtain a numerical estimate of the stiffness constant which is in a good agreement with the analytical prediction. The connection between the parameters in joint distribution function and the moments of height variables eliminates the arduous work of directly relating the parameters of joint distribution function to those of the total distribution function. We also directly measured the power spectrum of the height and obtained a value of the stiffness constant, which is very close to the analytic prediction and the estimate from the real-space coarse graining. This suggests that the measurement of the power spectrum might provide a simple route towards the construction of effective field theories. We also demonstrated that effective defect-defect interactions can be extracted from numerical studies of the defect-density power spectrum.

The compressible TIAFM [19,20] is currently being studied using these techniques. The effective field theory and defect-defect interactions in this model are of interest for the study of alloys with the elastic interactions, and for the study of glassy dynamics [6].

ACKNOWLEDGMENTS

This work was supported in part by the DOE Grant No. DE-FG02-ER45495. We would like to thank David Olmsted, Mike Ignatiev, and Mark Sobkowicz for helpful discussions, and Jane' Kondev for his insightful comments on the manuscript.

[1] G. H. Wannier, Phys. Rev. **79**, 357 (1950).
[2] B. Nienhuis, H. J. Hilhorst, and H. W. J. Blöte, J. Phys. A **17**, 3559 (1984).
[3] H. W. J. Blöte and M. P. Nightingale, Phys. Rev. B **47**, 15 046 (1993).
[4] K. Binder, Z. Phys. B: Condens. Matter **43**, 119 (1981).
[5] H. W. J. Blöte and H. J. Hilhorst, J. Phys. A **15**, L631 (1982).
[6] Lei Gu and B. Chakraborty, in *Structure and Dynamics of Glasses and Glass Formers*, edited by C. A. Angell, K. L. Ngai, J. Kieffer, T. Egami, and G. U. Nienhaus, MRS Symposia Proceedings No. 455 (Materials Research Society, Pittsburgh, 1997), p. 229; Lei Gu, Ph.D. thesis, Brandeis University, 1999.
[7] B. Chakraborty, Lei Gu, and Hui Yin, J. Phys. Condens. Matter (to be published).
[8] B. Nienhuis, *Phase Transitions and Critical Phenomena*, edited by C. Domb and J. L. Lebowitz (Academic Press, New York, 1987), Vol. 11.
[9] K. Kaski, K. Binder, and J. D. Gunton, J. Phys. A **16**, L623 (1983).
[10] K. Kaski, K. Binder, and J. D. Gunton, Phys. Rev. B **29**, 3996 (1984).
[11] R. J. Baxter, *Exactly Solved Models in Statistical Mechanics* (Academic Press, London, 1982).
[12] Chen Zeng and C. L. Henley, Phys. Rev. B **55**, 14 935 (1997).
[13] H. W. J. Blöte, M. P. Nightingale, X. N. Wu, and A. Hoogland, Phys. Rev. B **43**, 8751 (1991).
[14] J. Stephenson, J. Math. Phys. **5**, 1009 (1964); **11**, 413 (1970).
[15] Nigel Goldenfeld, *Lectures on Phase Transitions and the Renormalization Group* (Addison-Wesley Publishing Company, New York, 1992).
[16] Larger cell size L implies less cells for a given system size, thus less coarse-grained height variables $\{h_i\}$ to average over for each sampled MC configuration.
[17] P. M. Chaikin and T. C. Lubensky, *Principles of Condensed Matter Physics* (Cambridge University Press, New York, 1995).
[18] Cristopher Moore, Mats G. Nordahl, Nelson Minar, and Cosma Shalizi, Phys. Rev. E **60**, 5344 (1999).
[19] Z. Y. Chen and M. Kardar, J. Phys. C **19**, 6825 (1986).
[20] Lei Gu, B. Chakraborty, P. Garrido, Mohan Phani, and J. L. Lebowitz, Phys. Rev. B **53**, 11 985 (1996).